JACS
JOURNAL OF THE AMERICAN CHEMICAL SOCIETY
pubs.acs.org/JACS
Article

# Redesigned Hybrid Nylons with Optical Clarity and Chemical Recyclability

Robin M. Cywar, Nicholas A. Rorrer,[‖] Heather B. Mayes,[‖] Anjani K. Maurya,[‖] Christopher J. Tassone, Gregg T. Beckham, and Eugene Y.-X. Chen*

Cite This: https://doi.org/10.1021/jacs.1c12611
Read Online



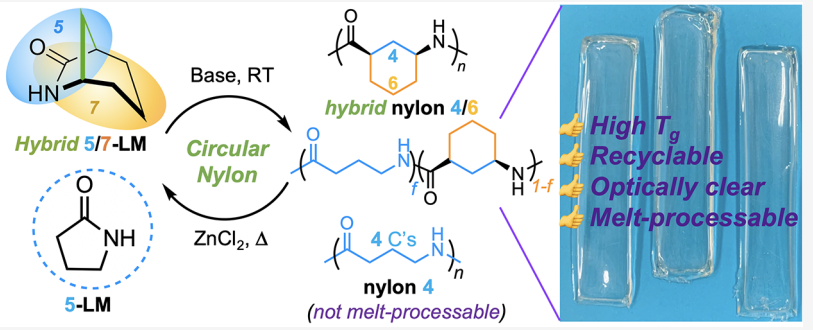


**ABSTRACT:** Aliphatic polyamides, or nylons, are typically highly crystalline and thermally robust polymers used in high-performance applications. Nylon 6, a high-ceiling-temperature (HCT) polyamide from ε-caprolactam, lacks expedient chemical recyclability, while low-ceiling temperature (LCT) nylon 4 from pyrrolidone exhibits complete chemical recyclability, but it is thermally unstable and not melt-processable. Here, we introduce a hybrid nylon, nylon 4/6, based on a bicyclic lactam composed of both HCT ε-caprolactam and LCT pyrrolidone motifs in a hybridized offspring structure. Hybrid nylon 4/6 overcomes trade-offs in (de)polymerizability and performance properties of the parent nylons, exhibiting both excellent polymerization and facile depolymerization characteristics. This stereoregular polyamide forms nanocrystalline domains, allowing optical clarity and high thermal stability, however, without displaying a melting transition before decomposition. Of a series of statistical copolymers comprising nylon 4/6 and nylon 4, a 50/50 copolymer achieves the greatest synergy in both reactivity and polymer properties of each homopolymer, offering an amorphous nylon with favorable properties, including optical clarity, a high glass transition temperature, melt processability, and full chemical recyclability.

## INTRODUCTION

Plastic waste accumulation requires solutions to enable circular material flows.[1−6] Besides the environmental consequences of plastic production and disposal, chiefly pollution, their disposal is an economic loss and contributes to further greenhouse gas emissions.[3,4,7] Circular life cycles are needed for both single-use and high-performance polymers, but current mechanical recycling typically results in reduced-quality products.[5,8−11] Nylons, or aliphatic polyamides (PAs), are used in textiles and engineering plastics, and are less commonly recycled.[12] Production of nylon 6 has a large carbon footprint and a host of other environmental issues.[7,13] As a choice material for fishing gear, nylons also comprise a substantial portion of the estimated ∼10% ocean plastic as lost or abandoned fishing gear, with nets contributing to >40% of the Great Pacific Garbage Patch.[14,15] Recent developments in biobased PAs address feedstock concerns and present advantageous properties such as tunable crystallinity or biocompatibility,[16−22] but end of life must also be considered for plastics.

Chemical recycling of polymers to monomers can regenerate virgin-quality polymers and reduce raw feedstock use.[5,23−26] However, highly exergonic polymerizations, or high-ceiling-temperature (HCT) systems, preclude selective monomer recovery for many commodity polymers.[11,24,27] Chemical recycling of nylon 6 to its monomer, HCT 7-membered ring lactam (7-LM or ε-caprolactam), has been demonstrated via several strategies, which exhibit challenges arising from the HCT, including selectivity to 7-LM and subsequent separations, need for using milder conditions, and obtaining 7-LM in a single step.[28−35] Designing for recyclability can circumvent such issues, but achieving requisite thermomechanical proper-

Received: December 1, 2021

ties for applications is a major challenge associated with the *redesign*[27] of synthetic polymers.[16,24,36] Increasing the ring strain of low-ceiling-temperature (LCT) monomers leads to increased ceiling temperature ($T_c$), providing a practical working range for polymerization and depolymerization, as well as improved material properties.[24,36,37] *Hybridization* has been recently established as an effective strategy to modulate thermodynamics and properties, wherein HCT and LCT monomers are fused into an atom-bridged, fused-ring offspring monomer.[27,36,38] This concept combines the polymerization capacity of the HCT parent while maintaining the facile depolymerization potential of the LCT parent. For example, the hybrid offspring monomer of five- and seven-membered ring lactones, [3.2.1] bicyclic lactone, produces a polyester with substantially improved properties than the parents.[36]

Nylon 4, from the five-membered lactam (5-LM), or 2-pyrrolidone, has attractive textile properties[39] and sustainability aspects including the ability to be biosourced,[40−43] biodegradability,[44−46] and chemical recyclability,[39,47] but it suffers in performance. Owing to a low $T_c$ of ∼70 °C in the bulk state,[48] the material undergoes concurrent melting and degradation (depolymerization), impeding melt processing. Despite significant efforts, nylon 4 was never commercialized using ring-opening polymerization.[39,49−51] This combination of conflicting thermal properties and recyclability is common for LCT polymers. Thus, it is of interest to explore *recyclable-by-design* lactam monomers in pursuit of desired, but otherwise conflicting, properties.

In this work, we extend the hybrid HCT/LCT monomer design concept to nylons through the fusion of 5-LM and 7-LM parents to the offspring [3.2.1] bicyclic lactam, 6-azabicyclo[3.2.1]octan-7-one, referred to here as 5/7-LM (Scheme 1). This lactam was first polymerized by Hall in

**Scheme 1. Hybridization of LCT 5-LM and HCT 7-LM Resulting in 5/7-LM, Which Was Hypothesized to Exhibit Synergistic De-/Polymerizability and Favorable Polymer Properties**

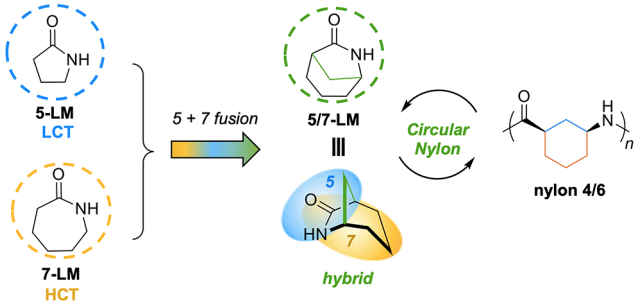


1958, for which characterization was not reported, but it was observed that the monomer was regenerated upon thermal degradation.[52] Our work here shows that 5/7-LM and the resulting hybrid nylon 4/6 have both high de-/polymerizability and substantially different properties than the parent polymers, nylon 4 and nylon 6. The unusual properties of nylon 4/6 provided an opportunity to understand the underlying structure−property relationships, which differ from the traditional PAs and analogous polyesters. To achieve a chemically recyclable nylon with useful properties, the copolymerization strategy[53] was utilized with the 5-LM + 5/7-LM pair, affording a nylon with synergistic properties that overcomes the limitations of each homopolymer.

## RESULTS

**Synthesis of Stereoregular Nylon 4/6 and Origin of Stereoselectivity.** The polymerization activity of 5/7-LM (a chiral monomer in its racemic (*RS*/*SR*)-(±) form, $^1$H and $^{13}$C NMR spectra: Figures S1 and S2) was studied using traditional anionic ring-opening (AROP) conditions for lactams (AROP mechanism: Scheme S1), including a strong base catalyst and an *N*-acyl-substituted activator derived from the 5/7-LM monomer, *N*-benzoyl-5/7-LM (NBzM, $^1$H and $^{13}$C NMR spectra: Figures S3 and S4) to facilitate initiation. The phosphazene superbase $^t$Bu-P$_4$, the *N*-heterocyclic carbene 1,3-dimesitylimidazol-2-ylidene (IMes), and the sodium adduct of the monomer (NaM) were compared as base catalysts at a [monomer]/[base]/[activator] ratio ([M]/[B]/[A]) of 50/1/1. Isolated yields of purified polymers are reported, which matched well with the conversion data when the reaction mixtures were analyzed in deuterated trifluoroacetic acid (TFA-*d*). Across all samples, there was no spectral evidence of isomerization to trans configuration in the polymer backbone (representative $^1$H and $^{13}$C NMR spectra: Figures S5 and S6). The structure of nylon 4/6 (Scheme 1) was confirmed by correlation spectroscopy and heteronuclear single quantum coherence 2D NMR (Figures S7 and S8); its Fourier transform infrared spectrum is shown in Figure S9.

Detailed results of 5/7-LM AROP behavior are presented in Table S1, showing the following general trends. Without an activator to provide a lower-energy initiation pathway (Scheme S1A,B), higher temperatures were required to produce nylon 4/6 (Table S1, entries 1−3). With the activator and $^t$Bu-P$_4$, room temperature (RT, ∼23 °C) and 60 °C provided good yields (Table S1, entries 4−8, 18), with the best yield of 95% achieved in *N*-methyl-2-pyrrolidone (NMP, 3.0 M in the monomer) at RT for 3 h. As shown in Figure 1, matrix-assisted laser desorption ionization−time-of-flight mass spectroscopy (MALDI-TOF MS) revealed a major and minor set of peaks for the samples produced at RT, 60, and 120 °C with $^t$Bu-P$_4$. Through end-group analysis (Figures S10 and S11), the minor peak sets were determined to represent self-initiated chains, while the major set represents activator-initiated chains, with both types bearing closed lactam chain ends (Figure 1).[54] The relative intensity of the minor peak set increases with temperature, in agreement with suppressed self-initiation at RT. However, polymerization at RT led to higher dispersities (*Đ*'s) than at higher temperatures. To study the molecular weights, gel-permeation chromatography (GPC) analysis was performed for select samples in hexafluoro-isopropanol (HFIP) (Table S2). GPC analysis revealed the number-average molecular weights ($M_n$) that were in agreement with those estimated by the [M]/[A] ratio and yield, as well as by the end-group analysis of $^1$H NMR spectra but relatively broad *Đ* (>2.0) for RT compared to higher temperatures (<2.0). This observation is presumably due to much slower initiation than propagation at RT, with the sample prepared at 120 °C displaying a unimodal elution profile (Figure S14). To reach higher $M_n$ by increasing the [M]/[A] ratio, use of $^t$Bu-P$_4$ and 120 °C was the most effective while maintaining [B] = 2.0 mol % (Table S2, entries 21−23).

For the effect of the base, NaM required more time to achieve comparable yields as with $^t$Bu-P$_4$ (Table S1, entries 11−16) due to higher basicity and solubility of $^t$Bu-P$_4$. On the other hand, NaM led to nylon 4/6 with the highest molecular weight and lowest dispersity of the series, $M_n$ = 48.7 kDa and



https://doi.org/10.1021/jacs.1c12611
J. Am. Chem. Soc. XXXX, XXX, XXX−XXX

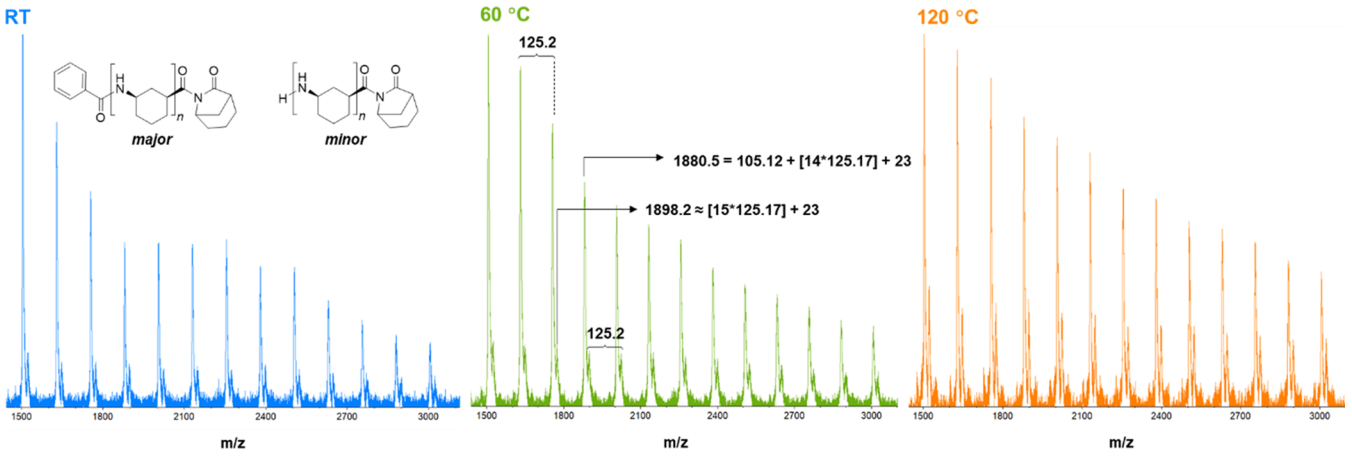


**Figure 1.** MALDI-TOF MS analysis of nylon 4/6 reveals a major and minor set of peaks corresponding to activator and self-initiated chains, respectively, for polymers produced at 50/1/1 [M]/[B]/[A] at different temperatures in NMP.

$Đ$ = 1.24 (Table S2, entry 23). IMes was also much slower compared to $^{t}$Bu-P$_4$, presumably due to the similar p$K_a$ values of IMes-H$^+$ and bicyclic lactams (p$K_a$ ≈ 24−25 in dimethyl sulfoxide).

In addition to 5/7-LM with the amide connected to the cyclohexyl ring at 1,3-positions, we also prepared the structural isomer 6/6-LM with the amide connected at the 1,4-positions (Figures S15 and S16). Using the same conditions as for 5/7-LM, the AROP of 6/6-LM produced low yields (<20%) of oligomers. Thus, the ring strain of 6/6-LM seems to be hardly affected by this ring fusion and behaves similarly to the nonstrained 6-LM parent (2-piperidone).

The stereoregularity of the resulting nylon 4/6 materials was analyzed by $^{13}$C NMR spectroscopy. Magnification of the carbonyl resonance region of the spectrum reveals the stereosequence information of the chiral monomer repeat units. Considering all possible, nonredundant triad stereosequences consisting of three repeat units exclusively in cis-configuration (i.e., no epimerization at the chiral centers), there are at least three possible carbonyl peaks (Scheme S2). For nylon 4/6 products from $^{t}$Bu-P$_4$, this region shows a predominant peak at 180.9 ppm in TFA-*d* with trace minor peaks (Figure 2A). This suggests a highly stereoregular polymer, which is confirmed by the chiral polymer prepared from the enantiopure monomer (−)-5/7-LM (Figures S17−S19, 2B), synthesized by chiral resolution crystallization.[55,56] End-group carbonyl peaks arise further away (175.5 and 185.1 ppm), and the minor peaks change with AROP conditions, indicating changes in tacticity (Figures S20−S22: effect of the base on tacticity; Figure S23: overlay). When NMP was used instead of THF with the $^{t}$Bu-P$_4$ catalyst, the minor peak was significantly reduced, and three peaks were observed in the IMes-catalyzed polymer product, appearing at 180.9, 180.7, and 180.6 ppm (Figure S22). The chiral polymers dissolved in TFA-*d* only at 55 °C for $^{13}$C NMR analysis and revealed a single carbonyl peak at 180.7 ppm (Figures 2B, S19).

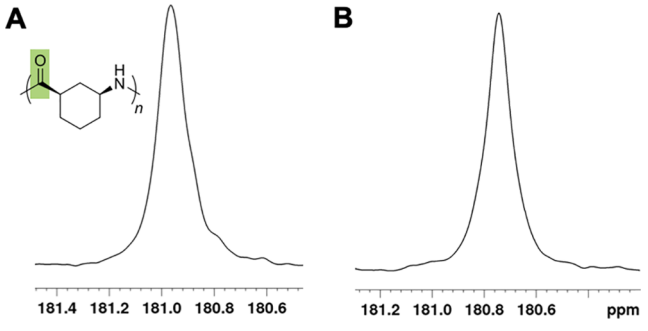


**Figure 2.** $^{13}$C NMR analysis (magnified carbonyl region, TFA-*d*) of nylon 4/6 produced with $^{t}$Bu-P$_4$ in NMP at RT from: (A) racemic (±)-5/7-LM and (B) chiral (−)-5/7-LM, recorded at 55 °C for solubility.

Next, we investigated the origins of stereoselectivity in the AROP of nylon 4/6. The fundamental step of propagation proceeds through attack of a bicyclic lactam monomer on the chain end by a bicyclic lactamate anion (Scheme S1C). Thus, we hypothesized that this sterically demanding, intermolecular addition provides stereoselectivity through *chain-end control* to produce *erythro*-disyndiotactic or *threo*-disyndiotactic nylon 4/6, corresponding to favored addition of the same or opposite enantiomer, respectively. To test the chain-end control hypothesis, we studied the polymerization behavior of (−)-5/7-LM. Substantially lower polymer yields were obtained: AROP at RT by $^{t}$Bu-P$_4$ in NMP yielded only 23% polymer, in stark contrast to the 95% obtained from the racemic monomer within the same period of 3 h (Table S1, entries 5 and 9). Likewise, a 54% yield was obtained from (−)-5/7-LM using NaM, NMP, at 60 °C, and in 24 h, versus 74% from the racemic monomer (Table S1, entries 14 and 15). The lower yield and slower kinetics suggest that the polymerization suffers when *erythro* is the only possible selectivity; therefore, *threo* attack is likely the more favorable scenario in the polymerization of (±)-5/7-LM.

Unlike the racemic nylon 4/6 products, the chiral materials derived from (−)-5/7-LM are insoluble in formic acid, HFIP, and TFA at RT, which is indicative of higher tacticity but complicated analysis. Optical rotation of the chiral samples was measured at RT in *m*-cresol. Although only cloudy solutions could be obtained, strong rotation of light was observed relative to the repeating unit: specific rotation, $[a]_D^{23}$, of (−)-*cis*-3-aminocyclohexane carboxylic acid = −12.0 ± 1.0° in *m*-cresol, $[a]_D^{23}$ of (−)-nylon 4/6 (Table S1, entry 10) = −177.9 ± 5.5° in *m*-cresol. This confirms highly enriched or complete *erythro*-disyndiotacticity. The large difference in the magnitude indicates that the chiral polymer also assumes a secondary structure in a dilute solution.[57] A higher standard deviation for the chiral polymer may be attributed to incomplete solubility.


https://doi.org/10.1021/jacs.1c12611
J. Am. Chem. Soc. XXXX, XXX, XXX−XXX

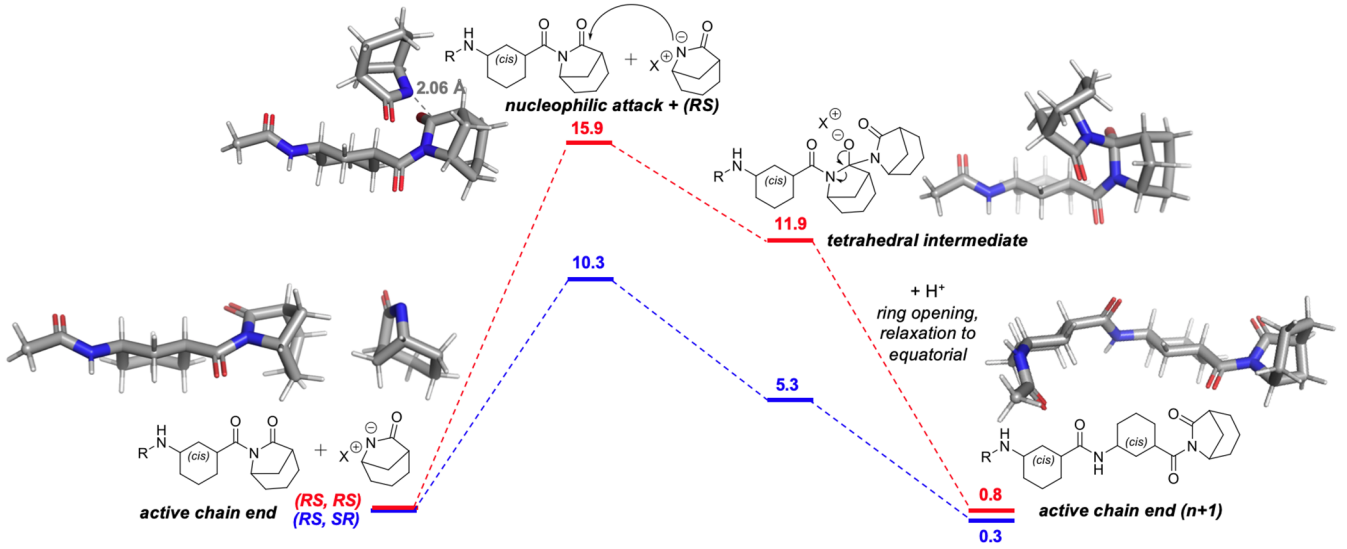


**Figure 3.** Free energy diagram comparing *RS* monomer addition to an *SR*-terminated chain (*threo*, blue) and *RS* monomer addition to an *RS*-terminated chain (*erythro*, red), with 3D representations of the low-energy conformations of model chains used in the density functional theory (DFT) calculations for *threo* addition. Values shown are the differences in Gibbs free energy at 100 °C for each reaction step compared to the Gibbs free energy of the reactants, in kcal mol$^{-1}$, calculated using DFT at the M06-2X2/Def2TZVP level of theory in implicit nitrobenzene (dielectric constant, $\varepsilon$ = 34.8).

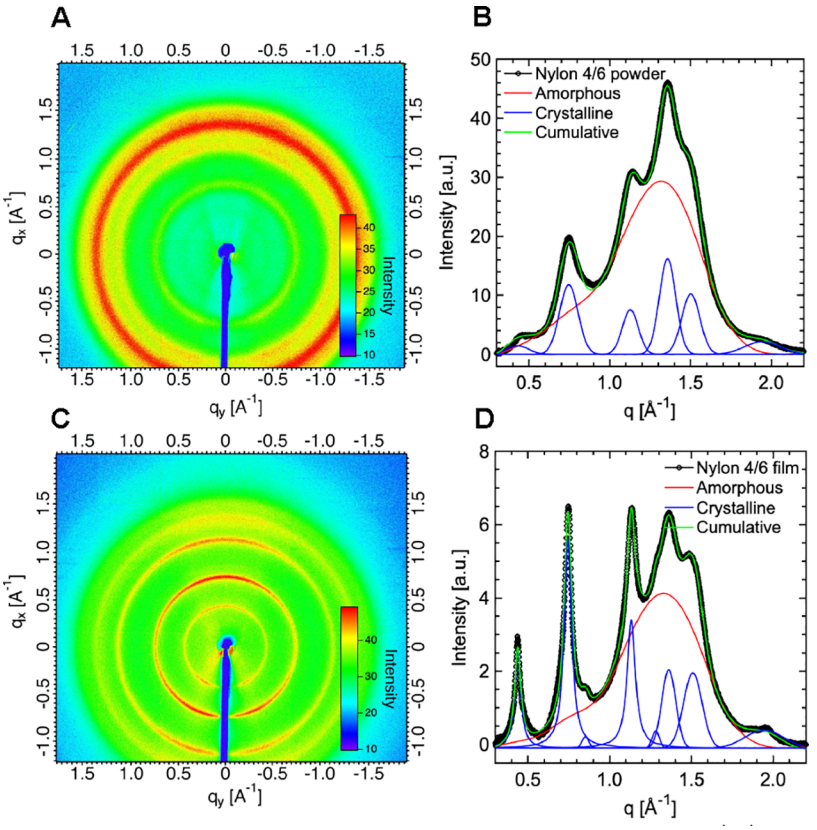


**Figure 4.** 2D-WAXS patterns of nylon 4/6 powder (A) and nylon 4/6 film (C) samples and 1D extracted radial profiles with fitting of amorphous and crystalline phases of powder (B) and film (D) samples.

To investigate which stereoselectivity is more kinetically favorable, DFT was used to model the propagation step. *Threo* and *erythro* addition of bicyclic lactamate anions to growing chains was modeled for each stereochemical and conformational scenario. For each stereochemical scenario [*RS* addition to *SR* (*threo*) and *RS* addition to *RS* (*erythro*)], propagation was modeled with the penultimate monomer in the axial and equatorial conformations for a total of four scenarios as the geometry of this unit could influence the sterics of monomer addition. While the bicyclic lactam is forced into axial conformation, it may relax to the equatorial after ring opening. Across all scenarios, the equatorial conformation for the



https://doi.org/10.1021/jacs.1c12611
J. Am. Chem. Soc. XXXX, XXX, XXX−XXX

penultimate monomer was found to be lower in energy, relaxing to the equatorial once protonated (Figure 3). *Threo* attack also was predicted to exhibit consistently lower $\Delta G^{\ddagger}$ energies: when comparing the addition of an *RS* monomer for *threo* versus *erythro* attack at 100 °C, the difference in the transition-state energies $\Delta\Delta G^{\ddagger} = 5.6$ kcal mol$^{-1}$ (Figure 3 and Table S4). These data, together with the observed low yields of an *erythro* polymerization, support selectivity to the *threo*-disyndiotactic polymer (i.e., alternating enantiomers along the chain) through an inherent *chain-end* control mechanism.

**Physical Properties of Nylon 4/6.** Like other PAs, nylon 4/6 was found to be soluble only in acidic solvents such as formic acid, TFA, HFIP, and *m*-cresol. Thermogravimetric analysis (TGA) of nylon 4/6 shows an onset decomposition temperature (5% mass loss), $T_{d,5}$, of 357 °C (Figure S24), followed by rapid decomposition and leaving zero residue. Neither a glass nor a melting transition ($T_g$ and $T_m$) was observed by differential scanning calorimetry (DSC) for powdered samples using varying heating and cooling rates (1, 10, and 40 °C/min) or by simultaneous DSC−TGA (SDT) (10 °C/min, Figure S25) through degradation. The chiral (−)-nylon 4/6 sample also did not show a $T_g$ or a $T_m$. Owing to a small change in the free volume during the transition, it is common for the $T_g$ of semicrystalline PAs and highly rigid polymers such as nylon 4/6 to go undetected by DSC. However, when this PA is heated through degradation at the bench, it does *not* enter viscous flow (liquify) above the $T_g$, as would be typical of an amorphous polymer. Thus, it came into question whether nylon 4/6 is amorphous or semicrystalline, possibly with a $T_m > T_d$ such that a $T_m$ was also not detectable by DSC.

Although a solvent-cast film was *colorless and transparent*, the wide-angle X-ray scattering (WAXS) patterns of nylon 4/6 powder and film samples showed that it is in fact semicrystalline (Figure 4B,D). The Scherrer equation was used to estimate average crystallite sizes from broadening of the fitted crystalline peaks, which were found to be ∼4.0 nm for the powder and ∼8.3 nm for the film (Table S3). Additionally, the nylon 4/6 film also showed evidence of the preferred orientation of polymer chains in the plane of the film along the growth direction (Figure 4C). Thus, the much smaller crystallites relative to the wavelength of visible light do not scatter it, resulting in an optically clear material[58]—an effect which was independent of $M_n$ prepared in this study (up to 48.7 kDa).

The nylon 4/6 film was brittle and could not be analyzed by dynamic mechanical analysis (DMA) for $T_g$ by the tan $\delta$ peak ($T_{g(DMA)}$). However, a $T_g$ at 176 °C was observed in a first DSC scan when the thin film sample was heated at 40 °C/min (Figure S26), but this first-scan phenomenon was difficult to reproduce. When repeated, the same film produced $T_g$-like signals at 146 and 199 °C during the first scans (Figures S27 and S28; all scans shown in Figure S29). We hypothesize that the $T_g$ could only be detected during the first heating scan of the film due to a higher free volume change for films combined with the release of moisture absorbed from the air (typical for PAs) during the transition, causing a detectable signal. A greater change in the free volume for the film is consistent with the higher degree of crystallinity (sharper peaks) and preferred orientation of polymer chains in the plane of the film observed by WAXS in the film compared to powder (Figure 4). Applying the Fox equation to a copolymer (vide infra) of 5/7-LM and 5-LM (using "dry" $T_{g(DMA)}$ of nylon 4 = 81 °C[59]) resulted in an estimated $T_g$ of ∼200 °C for nylon 4/6, which is consistent with the observed DSC $T_g$ values, considering that the DMA-determined $T_g$ values from tan $\delta$ peaks are typically higher than those observed by DSC and the observation that >150 °C was required to fully dry samples.

The thermodynamic parameters for 5/7-LM (equilibrium monomer concentration $[M]_{eq}$, enthalpic and entropic changes of polymerization ($\Delta H_p^{\circ}$, $\Delta S_p^{\circ}$), and $T_c$) were obtained from a van 't Hoff plot displaying $\ln[M]_{eq}$ as a function of $1/T$ (K) (Figure S30). The $[M]_{eq}$ values of parallel reactions ($[M]_{eq}$ = 0.96 M) were measured by LC−MS. The thermodynamic parameters were found to be $\Delta H_p^{\circ} = -10.0$ kJ mol$^{-1}$ and $\Delta S_p^{\circ} = -20.1$ J mol$^{-1}$ K$^{-1}$, with a calculated $T_c = 225$ °C at $[M]_0 = 1.0$ M. The $\Delta G_p$ values calculated by DFT are near zero at 25, 100, and 120 °C (Table S4), consistent with the $\Delta G_p$ values calculated at these temperatures using experimentally determined $\Delta H_p^{\circ}$ and $\Delta S_p^{\circ}$ values in the Gibbs free energy equation, including the trend of higher $\Delta G_p$, and thus decreasing the driving force, with increasing temperature. Given the near-zero $\Delta G_p$ values, polymer precipitation clearly plays a large role in driving the equilibrium polymerization forward.

**Chemical Recycling of Nylon 4/6.** To test the chemical recyclability of nylon 4/6 through depolymerization, high temperature and low vacuum were applied to the samples in a glass sublimator (Figure S31), allowing the condensation of recycling products for quantification and analysis. Thermolysis was conducted >400 °C, resulting in quantitative mass recovery but an impure 5/7-LM product (Figure S32). To reduce the recycling temperature and improve selectivity to the monomer, Lewis acid catalysis by $ZnCl_2$ was employed to activate carbonyls for amine backbiting. $ZnCl_2$ was chosen for its strong Lewis acidity, high thermal stability, and previously demonstrated success for catalyzed polyester depolymerization.[60] When 20 wt % is adsorbed to the polymer surface, the $T_{d,5}$ decreases by 51 °C, resulting in a smooth TGA decomposition profile (Figure S33). A heating mantle temperature of 290 °C with $ZnCl_2$ resulted in 93−98% mass recovery relative to the starting polymer over several trials (15−18 h), and a ring of the sublimate also condensed on the reactor walls (Figure S31), which was not combined with the product collected from the condenser. The crude product (Figure 5) was found to be in good purity (integrated $^1$H NMR spectrum: Figure S34) but contained Zn species which cosublimed, as well as a small fraction of the activator and impurities, which contributed to over-integration in the 1.50−

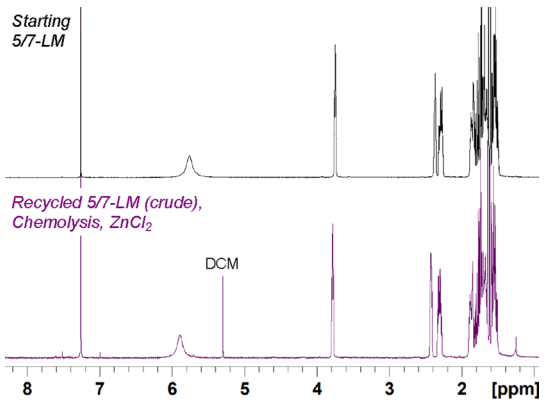


**Figure 5.** Starting monomer and crude, recovered monomer after chemolysis with 20 wt % $ZnCl_2$.



https://doi.org/10.1021/jacs.1c12611
J. Am. Chem. Soc. XXXX, XXX, XXX−XXX

**Table 1. Selected Results from the Copolymerization of 5-LM and 5/7-LM[a]**

| entry | 5-LM/5/7-LM | [M]/[B]/[A] | base | time (h) | yield (%) | % 5/7-LM incorp. | $M_{n,GPC}$[b] (kDa) | $Đ$[c] | $T_{d,5}$[d] (°C) |
|---|---|---|---|---|---|---|---|---|---|
| 1 | 100:0 | 50/1/1 | $^tBuP_4$ | 1.5 | 78 | n/a | 5.00 | 1.64 | 291 |
| 2 | 95:5 | 50/1/1 | $^tBuP_4$ | 1.5 | 77 | 7 | 3.56 | 1.28 | 296 |
| 3 | 85:15 | 50/1/1 | $^tBuP_4$ | 1.5 | 75 | 17 | 5.32 | 1.11 | 298 |
| 4 | 85:15 | 50/1/1 | NaSLM | 1.5 | 59 | 20 | 6.27 | 1.29 | n.d. |
| 5 | 75:25 | 50/1/1 | $^tBuP_4$ | 1.5 | 77 | 30 | 3.61 | 1.13 | 304 |
| 6 | 50:50 | 50/1/1 | $^tBuP_4$ | 1.5 | 41 | 54 | 7.19 | 1.08 | 322 |
| 7 | 15:85 | 50/1/1 | $^tBuP_4$ | 1.5 | 90 | 90 | 9.15 | 1.36 | 355 |
| 8 | 100:0 | 250/5/1 | NaSLM | 24 | 53 | 0 | 17.8 | 2.52 | 297 |
| 9 | 85:15 | 250/5/1 | NaSLM | 24 | 64 | 15 | 18.7 | 1.37 | 307 |
| 10 | 75:25 | 250/5/1 | NaSLM | 24 | 58 | 25 | 27.5 | 1.33 | 310 |
| 11 | 50:50 | 250/5/1 | NaSLM | 24 | 71 | 48 | 22.3 | 1.49 | 338 |
| 12 | 50:50 | 250/5/1 | NaSLM | 24 | 93 | 51 | 25.1 | 1.22 | 338 |
| 13 | 15:85 | 250/5/1 | NaSLM | 24 | 49 | 80 | 25.4 | 1.53 | 350 |
| 14 | 50:50 | 500/10/1 | NaSLM | 24 | 66 | 50 | 59.8 | 1.30 | 329 |
| 15 | 50:50 | 1000/20/1 | NaSLM | 24 | 25 | 45 | 40.7 | 1.37 | 326 |

[a]Entries 1−7 were performed with 250−500 mg of total monomers, entries 8−11 and 13 were performed with 2−3 g, and entry 12 was performed with 10 g; n/a = not applicable; n.d. = not determined. [b]Absolute molecular weight using a GPC system equipped with multiangle light scattering and refractive index detectors using HFIP as the eluent and assuming 100% mass recovery. [c]Dispersity determined using a GPC system equipped with multiangle light scattering and refractive index detectors using HFIP as the eluent and assuming 100% mass recovery. [d]Determined by TGA immediately after drying the samples in a 100 °C vacuum oven.

2.36 ppm region. A trial with 10 wt % $ZnCl_2$ resulted in the same yield but required longer time to complete (21 h). Resubliming the monomer at 55 °C and filtering off insoluble particles with diethyl ether resulted in pure 5/7-LM (integrated spectrum: Figure S35) in 70% isolated yield, which repolymerized identically to a control with the fresh monomer (NaM/60 °C/24 h, 75% yield for both). A control in which nylon 4/6 without $ZnCl_2$ was held at 290 °C overnight resulted in no monomer recovery, demonstrating the importance of catalysis in the chemical recycling of this nylon.

**Synergies of the Copolymers of Nylon 4/6 and Nylon 4.** Considering the high recyclability but the nonmelt processability (low thermal stability) of nylon 4 and the balanced de-/polymerizability, high thermal stability, and optical clarity of nylon 4/6, we were intrigued by the possibility of developing copolymers of nylons 4 and 4/6. To this end, we investigated the copolymerization of 5-LM and 5/7-LM (Table 1), performed at RT. For mixtures containing over 75 mol % 5-LM, no solvent was required, and with ≥50% 5/7-LM, minimal NMP was used to dissolve the monomers for a high-concentration polymerization (30−60 M). At the outset, a 50/1/1 $[M_{tot}]/[B]/[A]$ ratio was applied with the $^tBu$-$P_4$ catalyst to obtain a spectrum of copolymer compositions, with the 5/7-LM incorporation ranging from 0 to 90% (Table 1, entries 1−7). All reactions solidified within 1 min, including the 5-LM homopolymerization, and isolated yields up to 90% were obtained. Incorporation of 5/7-LM, determined by $^1H$ NMR spectroscopy, tracked well with the monomer feed ratios for both the 50/1/1 and 250/5/1 ratios (Figures S36−S46) as similar conversions were reached for both monomers when checked. The $^{13}C$ NMR spectra showed sequence distributions consistent with a statistical copolymer and a loss of chain end-controlled stereoselectivity for the 5/7-LM units (Figures S48−S50). The observed unimodal TGA decomposition profiles are also consistent with a statistical copolymer structure (Figures S51−S64). The copolymerization was then scaled up to a 250/5/1 [M]/[B]/[A] ratio and 2−3 g total monomers using NaSLM, all solidifying within 10 min, but left to continue polymerizing for 24 h. Although $^tBu$-$P_4$ provided narrower $Đ$ copolymers, sodium is a more economical base. The higher [M]/[A] ratio was successful in producing $M_n$ > 15 kDa for all copolymer compositions, enabling reliable thermomechanical characterizations. When the 50:50 monomer ratio was scaled up to 10 g monomers, the highest isolated copolymer yield of 91% was obtained. A 50/50 copolymer with $M_n$ = 59.8 kDa was also prepared by increasing [M]/[B]/[A] to 500/10/1 (Table 1, entry 14). Across all copolymerization runs, narrower $Đ$ values (1.08−1.49) were obtained for the copolymers relative to each homopolymer prepared under the same conditions (GPC traces: Figures S65−S69).

Nylon 4 and nylon 4/6-*co*-nylon 4 samples produced at the 50/1/1 ratio were analyzed by SDT (Figures S70−S72) to visualize the proximity of melting and onset degradation. Nylon 4 melting ($T_{m(SDT)}$ = 258 °C) is concurrent with onset degradation ($T_{d,5(SDT)}$ = 263 °C). When 17% 5/7-LM is incorporated, the $T_{m(SDT)}$ decreases to 245 °C and the heat flow curve returns to the baseline briefly before onset decomposition at $T_{d,5(SDT)}$ = 276 °C. At 54% 5/7-LM incorporation, a small endotherm is present just above 200 °C with a $T_{d,5(SDT)}$ = 309 °C. This gain in thermal stability is exactly the average of the two parent $T_{d,5(SDT)}$ values. The trend of increased $T_d$ and widened processing window is illustrated by the overlaid SDT curves in Figure S73. The highest $T_{d,5}$ values were obtained by TGA, immediately after drying the samples in a 100 °C vacuum oven (Table 1).

Relative to nylon 4, crystallinity was reduced at ∼15 and ∼25% 5/7-LM incorporations and essentially eliminated above ∼50%, for which no thermal transitions were observed after the first DSC heating scans (Figures S74−S81). The low $M_n$ copolymer with ∼50% 5/7-LM incorporation showed a first-scan endotherm at 204 °C (Figure S77), but this was not observed for the higher $M_n$ copolymers with ∼50% 5/7-LM incorporation (Figures S78−S80). Like the homopolymers, the copolymer $T_g$ signals were not reliably detectable by DSC.

To further probe thermal stability, the spectrum of copolymers made at the 250/5/1 ratio was subjected to 1 h isothermal holds at theoretical processing temperatures (Figure



https://doi.org/10.1021/jacs.1c12611
J. Am. Chem. Soc. XXXX, XXX, XXX−XXX

6). Incorporation of 5/7-LM clearly increases the thermal stability of the nylon 4 copolymers. Specifically, an isothermal hold of nylon 4 at its $T_m$ (258 °C) for 1 h results in ~80% loss by weight due to thermal degradation. It was difficult to gauge a true processing temperature for the amorphous ~50% 5/7-LM compositions by DSC alone; however, a sample was observed to liquify on a hot surface at ~230 °C. It showed enhanced stability at 250 °C, losing only ~9% weight after 1 h, including water weight. After 1 h at 230 °C, only 4% was lost (Figure S82). As expected, the copolymer with a higher 5/7-LM incorporation of 80% shows higher thermal stability at 250 °C, with negligible mass loss after 1 h.

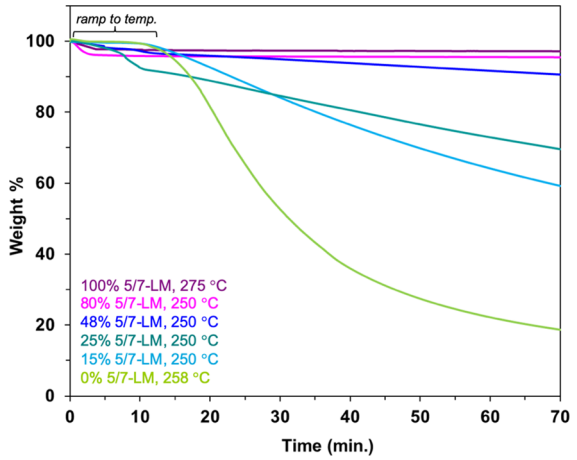


**Figure 6.** Isothermal holds of copolymers of varying compositions at processing-relevant temperatures for 1 h.

To verify that the covalently bound copolymer structure was responsible for the increase in thermal stability, a 50:50 physical blend of nylon 4 and nylon 4/6 was prepared by solvent casting. The two homopolymers were in fact *immiscible*, creating a cloudy solution and phase-separating upon drying, while ~50/50 nylon 4/6-*co*-nylon 4 of the develops a homogeneous and optically clear film (Figure 7, inset). The TGA profile of the physical blend shows a two-step decomposition profile, corresponding to the individual components in the blend, whereas the copolymer displays a single, narrow decomposition profile (Figure 7).

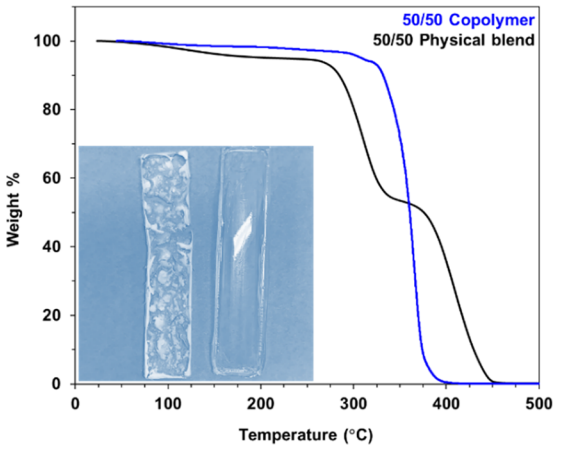


**Figure 7.** TGA profiles of a physical blend of 50/50 nylon 4/6 and nylon 4 compared to the ~50/50 statistical copolymer. Inset: solvent-cast thin films with the physical blend on the left and the copolymer on the right (the white streak is a reflection of light).

Thin films for DMA were prepared from the samples produced at the 250/5/1 ratio. A decrease in crystallinity is visually apparent (Figure S86), with the copolymer of 48% 5/7-LM composition becoming optically clear and amorphous (WAXS analysis: Figure S87). Nylon 4 thin films were too brittle and failed during testing but were found to have a dry $T_{g(DMA)}$ = 81 °C.[59] Water-dependent shifts in the tan $\delta$ curve (the ratio of loss to storage moduli), typical for nylons, were also observed for the copolymers. The air-equilibrated samples show lower tan $\delta$ peak values ($T_{g(DMA)}$) in the first heating scan, followed by an increase in the storage modulus and higher $T_{g(DMA)}$ during the second heating scan, representing the dry $T_{g(DMA)}$. For the 48% 5/7-LM composition, the two $T_{g(DMA)}$ values are 76 °C apart at 80 and 156 °C (Figure 8A,B). For 25% 5/7-LM, the $T_{g(DMA)}$ values are only 15 °C apart at 85 and 100 °C (Figures S88 and S89). The overall low tan $\delta$ intensities are indicative of stiff materials. The copolymer with 48% 5/7-LM also exhibits a rubbery plateau above the $T_g$ for both heating scans, uncommon for amorphous materials of low to medium $M_n$. Curiously, the storage modulus of the 25% 5/7-LM composition is about an order of magnitude lower than that of the 48% 5/7-LM copolymer and nylon 6 (Figure S90) at RT. Tensile analysis of the ~50/50 nylon 4/6-*co*-nylon 4 thin films shows a high Young modulus (2.28 ± 0.38 GPa), an ultimate stress of 54 ± 5 MPa, an elongation at ultimate stress of 4.4 ± 1.3%, and an elongation at break of 2.4−13.4% (Figure S91 and Table S5); the stress−strain curve shown in Figure 8C best represents the average data. The high Young modulus is also comparable to that of nylon 6.[61]

Water absorption behavior was also measured by submerging films for 24 h (Figure S92). The 48% 5/7-LM copolymer absorbed a similar amount of water to nylon 4 (28 and 23%, respectively), and both became more flexible owing to plasticization by water. The 15% composition unexpectedly absorbed 53% of its original mass, becoming soft and tearing apart while it was immersed. These differences across thermal stabilities, storage moduli, and water uptake behavior further highlight the synergy of a ~50/50 composition.

Chemical recycling of the ~50/50 copolymer samples was conducted using 10 wt % $ZnCl_2$ adsorbed to the polymer powder. TGA of the $ZnCl_2$−copolymer mixture showed a 71 °C drop in $T_{d,10}$ (Figure S93) to 264 °C, at which the polymer is liquified. In practice, a sublimator with a cryogenic condenser at −78 °C (5-LM melting point = 24 °C) and external mantle temperature = 300 °C were required. Quantitative monomer recovery relative to the starting polymer mass was obtained after 3 h, and the crude product was pure with a nearly identical ratio of 5/7-LM to 5-LM monomers as the starting polymer (integrated spectrum: Figure S94) but likely contained some Zn species (NMR silent). The crude recycling product (Figure 9) crystallized upon cooling under a layer of pentane. After decanting, small impurity peaks in the $^1$H NMR spectrum were reduced, however with a slight loss of 5/7-LM (integrated spectrum: Figure S95).

## DISCUSSION

Monomer design through HCT/LCT monomer hybridization aims to achieve the high polymerizability of the HCT parent while maintaining the selective recyclability of the LCT parent, thereby overcoming property trade-offs in a single monomer


https://doi.org/10.1021/jacs.1c12611
J. Am. Chem. Soc. XXXX, XXX, XXX−XXX

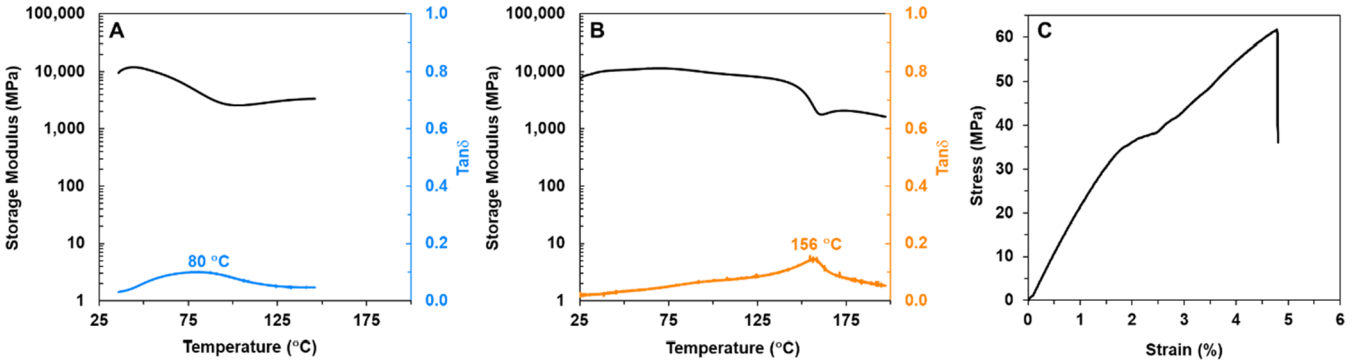


**Figure 8.** Thermomechanical analysis of the ~50/50 nylon 4/6-*co*-nylon 4 thin films. (A) First heating scan of DMA at 5 °C/min, 1 Hz; (B) second heating scan of DMA at 5 °C/min, 1 Hz; (C) representative stress−strain curve (RT, 5 mm/min).

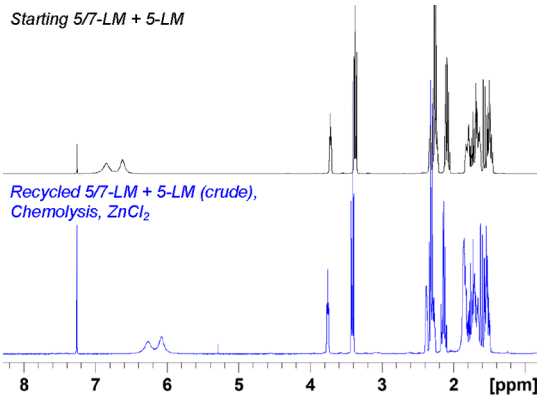


**Figure 9.** Starting monomers and crude, recycled monomers after chemolysis with 10 wt % $ZnCl_2$.

structure. In this work, the chemically recyclable hybrid 5/7-LM shows good polymerization activity in solution across the tested temperature range from RT to 120 °C, across which each parent polymer would face an activity cutoff due to $T_c$. The experimentally determined negative $\Delta H_p^\circ$ and $\Delta S_p^\circ$ values are consistent with strained ring monomers exhibiting thermodynamic reversibility (i.e., moderate $T_c$ values)[24,27] and with a $\Delta H_p^\circ$ between those reported for 5-LM and 7-LM.[48] Racemic 5/7-LM polymerization exhibits chain-end controlled stereoselectivity to *threo*-disyndiotactic nylon 4/6, but its high tacticity does not result in high crystallinity.

The unique physical properties of nylon 4/6 provided an opportunity to understand the underlying structure−property relationships for both fundamental understanding and for the benefit of future hybrid monomer design. Nylon 4/6 is a highly stereoregular, semicrystalline PA with nanocrystalline domains which result in optical clarity, but melt processing is prevented by a $T_m$ above the $T_d$. Most PAs and stereoregular polymers tend to be (visibly) semicrystalline, and both a PA and polyester analogue to nylon 4/6 are semicrystalline with a $T_m$ below the $T_d$. Interestingly, the PA analogue, from the ring opening of 8-oxa-6-azabicyclo[3.2.1]octan-7-one, which contains an ether bond between C1 and C3 in the resulting polymer backbone, exhibits a $T_m$ close to $T_d$.[62−64] Besides nylon 4 and nylon 4/6, other PAs with $T_m \geq T_d$ include polyaramides (e.g., Nomex)[65] and polypeptides.[66]

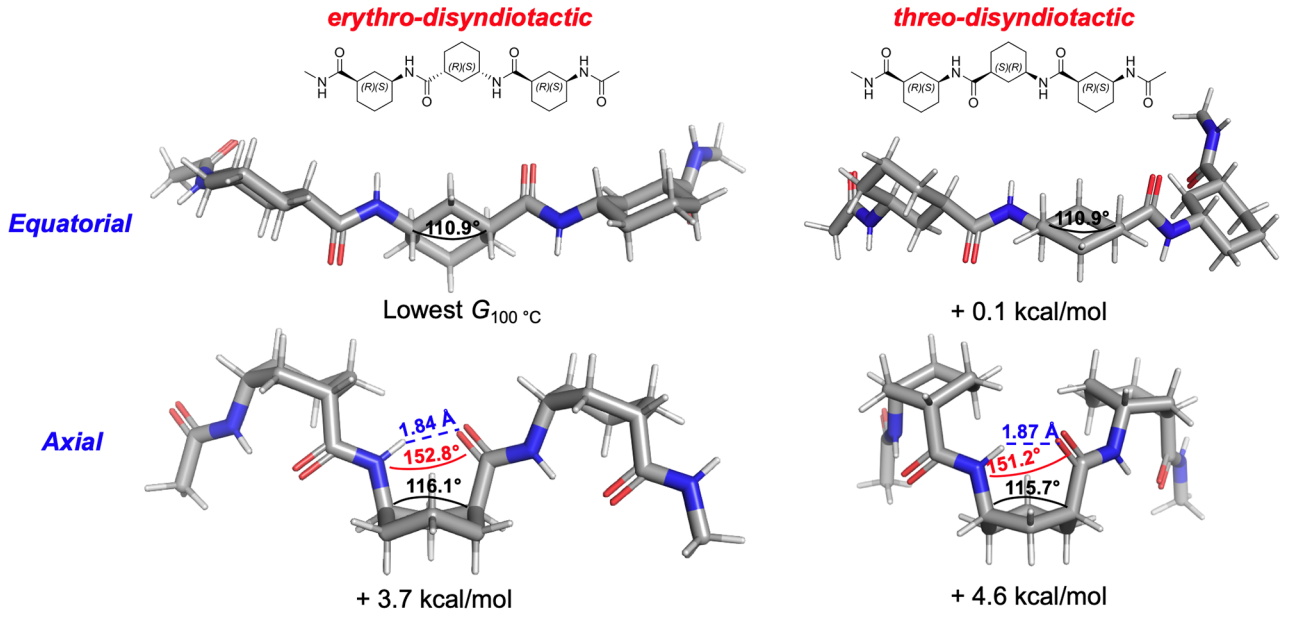


**Figure 10.** Lowest energy conformations and relative free energy differences for representative nylon 4/6 trimers, calculated with DFT at the M06-2X2/Def2TZVP level of theory in implicit nitrobenzene at 100 °C.



https://doi.org/10.1021/jacs.1c12611
J. Am. Chem. Soc. XXXX, XXX, XXX−XXX

To gain insight into chain conformation and rationalize the physical properties of nylon 4/6, DFT was employed to model the lowest-energy conformations of representative nylon 4/6 trimers with 2° amide end groups (Figure 10). Each 1,3-*cis*-cyclohexyl unit of the backbone can assume a diaxial or diequatorial conformation, and in the axial conformation, 1,3 C═O and −NH are in close proximity. Diaxial interactions, which are usually destabilizing, could be more favorable here due to formation of a H-bond. For both *threo*- and *erythro*-disyndiotactic trimers, the equatorial conformations were found to be 3.7−4.6 kcal $mol^{-1}$ lower in free energy than their axial conformations at 100 °C (Figure 10). In the axial conformations, the lowest-energy rotamers aligned the amide hydrogen toward the oxygen to enable H-bonding. However, this intramonomer H-bond N−H−O angle is 151−153°, far from the ideal 180°, while the O−H distance is extremely close at 1.84−1.87 Å (typical H-bond lengths are ∼2.0−3.0 Å). The stabilizing contribution of this weak H-bond is insufficient to offset the strain of the diaxial steric interactions, which perturb the angle of the C1−C2−C3 ring bond from the ideal 109.5° for this $sp^3$ bond to ∼116°, with other angles also being strained to a lesser extent (Figure S90). Taking into account these energetic differences, a Boltzmann distribution of conformations at 27 °C would be ∼800:1 equatorial/axial, ∼150:1 at 127 °C, ∼50:1 at 227 °C, and ∼1.2:1 at 327 °C.

From this information, we hypothesize that nylon 4/6 thermal decomposition (recycling) occurs before melting due to this conformational change and *intramonomer* H-bonding. This conformation change, occurring in the amorphous regions at high temperatures, mirrors the positioning of bonds in the bicyclic 5/7-LM, facilitating ring closing for recycling through a lower-energy pathway than that required to melt the crystallites.

To capitalize on the advantageous properties of nylon 4/6, we pursued nylon 4-based copolymers. Nylon 4 has conflicting performance and recyclability properties due to its LCT, which is unfortunate considering several sustainable features (bio-based monomer, chemically recyclable, biodegradable). Regarding the synthesis of 5/7-LM, the precursor *m*-aminobenzoic acid has been recognized as a valuable bioproduct.[67] Besides obtaining the desired statistical copolymer microstructure, 5/7-LM and 5-LM showed synergistic reactivity and properties relative to the parent homopolymers, which were immiscible. Increasing content of 5/7-LM improves the thermal stability of nylon 4 copolymers, and although the ∼15 and ∼25% 5/7-LM compositions show improved stability and are semicrystalline, they are likely not stable enough for melt processing and are also softer materials. In contrast, the ∼50/50 nylon 4/6-*co*-nylon 4 composition (Figure 11) is a strong, stiff, amorphous, optically clear, and thermally stable PA exhibiting a rubbery plateau, suggesting that adequate H-bonding is present despite a lack of crystallites.


**Figure 11.** Photographs of thin films of nylon 4/6-*co*-nylon 4 in ∼50/50 composition. The bottle logo is a trademark owned by Alliance for Sustainable Energy, LLC, and used with permission.

The enhanced thermal stability and thermomechanical properties of the ∼50/50 copolymer are thus promising for processing techniques such as injection molding or melt spinning. The material readily absorbs atmospheric moisture, important for textiles, and with both "ambient" and "dry" $T_{g(DMA)}$ values 40−100 °C higher than those of nylon 6. In addition to typical nylon applications such as fibers, this material could be potentially used for clear coatings and composites, with the same solvent resistance as typical nylons but higher temperature resistance. Moreover, chemical recyclability could enable the recovery of both components of composites, for example, carbon fiber materials.

Future work on this copolymer includes study of the effect of chain end caps (both initiating and terminating),[47,50,68] thermal stabilizers, and plasticizers on thermomechanical and rheological properties to further improve processing stability. For larger-scale recycling, we envision a depolymerization process where a liquified polymer is passed over a fixed catalyst bed and the reformed comonomer products are immediately condensed. Furthermore, as nylon 4 has been found to biodegrade in soil and marine environments[44,45] and nylon 4/6 also has a four-carbon backbone, the biodegradation of ∼50/50 nylon 4/6-*co*-nylon 4 is under long-term study. The exploration of additional hybridized lactams, including those resulting from different ring fusions or containing multiple functionalities, merits continued investigation.

## ■ ASSOCIATED CONTENT

### Supporting Information

The Supporting Information is available free of charge at https://pubs.acs.org/doi/10.1021/jacs.1c12611.

Details of instruments, experimental and computational procedures, additional figures, photographs, tables, and DFT-optimized Cartesian coordinates (PDF)

## ■ AUTHOR INFORMATION

### Corresponding Author

**Eugene Y.-X. Chen** − *Department of Chemistry, Colorado State University, Fort Collins, Colorado 80523-1872, United States;* orcid.org/0000-0001-7512-3484; Email: eugene.chen@colostate.edu

### Authors

**Robin M. Cywar** − *Department of Chemistry, Colorado State University, Fort Collins, Colorado 80523-1872, United States; Renewable Resources and Enabling Sciences Center, National Renewable Energy Laboratory, Golden, Colorado 80401, United States*

**Nicholas A. Rorrer** − *Renewable Resources and Enabling Sciences Center, National Renewable Energy Laboratory, Golden, Colorado 80401, United States;* orcid.org/0000-0001-9134-5853

**Heather B. Mayes** − *Renewable Resources and Enabling Sciences Center, National Renewable Energy Laboratory, Golden, Colorado 80401, United States;* orcid.org/0000-0001-9373-0106

**Anjani K. Maurya** − *SLAC National Accelerator Laboratory, Stanford Synchrotron Radiation Lightsource, Menlo Park, California 94025, United States*

**Christopher J. Tassone** − *SLAC National Accelerator Laboratory, Stanford Synchrotron Radiation Lightsource, Menlo Park, California 94025, United States*

**Gregg T. Beckham** − *Department of Chemistry, Colorado State University, Fort Collins, Colorado 80523-1872, United States; Renewable Resources and Enabling Sciences Center, National Renewable Energy Laboratory, Golden, Colorado 80401, United States;* orcid.org/0000-0002-3480-212X

Complete contact information is available at: https://pubs.acs.org/10.1021/jacs.1c12611

### Author Contributions

[‖]N.A.R., H.B.M., and A.K.M. equal contributors.

### Notes

The authors declare no competing financial interest.

## ■ ACKNOWLEDGMENTS

This work was supported by the U.S. Department of Energy, Office of Energy Efficiency and Renewable Energy (EERE), Advanced Manufacturing Office (AMO), and Bioenergy Technologies Office (BETO). This work was performed as part of the BOTTLE Consortium, which includes the members from Colorado State University, and funded under contract no. DE-AC36-08GO28308 with the National Renewable Energy Laboratory. Computational work was sponsored by the EERE and also used the Extreme Science and Engineering Discovery Environment (XSEDE),[69] which is supported by the National Science Foundation grant number ACI-1548562 through allocation TG-MCB170097. Use of the Stanford Synchrotron Radiation Lightsource, SLAC National Accelerator Laboratory, is supported by the U.S. Department of Energy, Office of Science, Office of Basic Energy Sciences under contract no. DE-AC02-76SF00515. We thank A. Westlie of the Chen group, W. Michener, J. Miscall, and B. Buss of the NREL for assistance with polymer analysis and R. Allen of the NREL for insightful discussions. We also thank S. A. Hesse and C. J. Takacs of the SLAC for beamtime support.

## ■ REFERENCES

(1) Law, K. L.; Narayan, R. Reducing environmental plastic pollution by designing polymer materials for managed end-of-life. *Nat. Rev. Mater.* **2022**, *7*, 104−116.

(2) Sheldon, R. A.; Norton, M. Green chemistry and the plastic pollution challenge: towards a circular economy. *Green Chem.* **2020**, *22*, 6310−6322.

(3) Hong, M.; Chen, E. Y.-X. Future Directions for Sustainable Polymers. *Trends Chem.* **2019**, *1*, 148−151.

(4) MacArthur, D. E.; Waughray, D.; Stuchtey, M. R. *The New Plastics Economy—Rethinking the Future of Plastics*; World Economic Forum, Ellen MacArthur Foundation and McKinsey & Company, 2016.

(5) Rahimi, A.; García, J. M. Chemical recycling of waste plastics for new materials production. *Nat. Rev. Chem.* **2017**, *1*, 0046.

(6) Hundertmark, T.; Mayer, M.; McNally, C.; Simons, T. J.; Witte, C. How plastics waste recycling could transform the chemical industry, 2018. https://www.mckinsey.com/industries/chemicals/our-insights/how-plastics-waste-recycling-could-transform-the-chemical-industry# (accessed August 9, 2021).

(7) Nicholson, S. R.; Rorrer, N. A.; Carpenter, A. C.; Beckham, G. T. Manufacturing energy and greenhouse gas emissions associated with plastics consumption. *Joule* **2021**, *5*, 673−686.

(8) Payne, J.; Jones, M. D. The Chemical Recycling of Polyesters for a Circular Plastics Economy: Challenges and Emerging Opportunities. *ChemSusChem* **2021**, *14*, 4041.

(9) Worch, J. C.; Dove, A. P. 100th Anniversary of Macromolecular Science Viewpoint: Toward Catalytic Chemical Recycling of Waste (and Future) Plastics. *ACS Macro Lett.* **2020**, *9*, 1494−1506.

(10) Garcia, J. M.; Robertson, M. L. The future of plastics recycling. *Science* **2017**, *358*, 870−872.

(11) Lange, J.-P. Managing Plastic Waste−Sorting, Recycling, Disposal, and Product Redesign. *ACS Sustainable Chem. Eng.* **2021**, *9*, 15722−15738.

(12) Hole, G.; Hole, A. S. Improving recycling of textiles based on lessons from policies for other recyclable materials: A minireview. *Sustain. Prod. Consum.* **2020**, *23*, 42−51.

(13) Bradford, S.; Rupf, R.; Stucki, M. Climbing Ropes-Environmental Hotspots in Their Life Cycle and Potentials for Optimization. *Sustainability* **2021**, *13*, 707.

(14) Macfadyen, G.; Huntington, T.; Cappell, R. Abandoned, Lost or Otherwise Discarded Fishing Gear. *UNEP Regional Seas Reports and Studies*, 2009; p 185.

(15) Lebreton, L.; Slat, B.; Ferrari, F.; Sainte-Rose, B.; Aitken, J.; Marthouse, R.; Hajbane, S.; Cunsolo, S.; Schwarz, A.; Levivier, A.; Noble, K.; Debeljak, P.; Maral, H.; Schoeneich-Argent, R.; Brambini, R.; Reisser, J. Evidence that the Great Pacific Garbage Patch is rapidly accumulating plastic. *Sci. Rep.* **2018**, *8*, 4666.

(16) Cywar, R. M.; Rorrer, N. A.; Hoyt, C. B.; Beckham, G. T.; Chen, E. Y.-X. Bio-based polymers with performance-advantaged properties. *Nat. Rev. Mater.* **2022**, *7*, 83−103.

(17) Stockmann, P. N.; Van Opdenbosch, D.; Poethig, A.; Pastoetter, D. L.; Hoehenberger, M.; Lessig, S.; Raab, J.; Woelbing, M.; Falcke, C.; Winnacker, M.; Zollfrank, C.; Strittmatter, H.; Sieber, V. Biobased chiral semi-crystalline or amorphous high-performance polyamides and their scalable stereoselective synthesis. *Nat. Commun.* **2020**, *11*, 509.

(18) Johnson, C. W.; Salvachua, D.; Rorrer, N. A.; Black, B. A.; Vardon, D. R.; St John, P. C.; Cleveland, N. S.; Dominick, G.; Elmore, J. R.; Grundl, N.; Khanna, P.; Martinez, C. R.; Michener, W. E.; Peterson, D. J.; Ramirez, K. J.; Singh, P.; VanderWall, T. A.; Wilson, A. N.; Yi, X.; Biddy, M. J.; Bomble, Y. J.; Guss, A. M.; Beckham, G. T. Innovative Chemicals and Materials from Bacterial Aromatic Catabolic Pathways. *Joule* **2019**, *3*, 1523−1537.

(19) Winnacker, M. Pinenes: Abundant and Renewable Building Blocks for a Variety of Sustainable Polymers. *Angew. Chem., Int. Ed.* **2018**, *57*, 14362−14371.

(20) Winnacker, M.; Rieger, B. Biobased Polyamides: Recent Advances in Basic and Applied Research. *Macromol. Rapid Commun.* **2016**, *37*, 1391−1413.

(21) Chen, J.; Dong, Y.; Xiao, C.; Tao, Y.; Wang, X. Organocatalyzed Ring-Opening Polymerization of Cyclic Lysine Derivative: Sustainable Access to Cationic Poly(ε-lysine) Mimics. *Macromolecules* **2021**, *54*, 2226−2231.

(22) Li, M.; Tao, Y. Poly(ε-lysine) and its derivatives via ring-opening polymerization of biorenewable cyclic lysine. *Polym. Chem.* **2021**, *12*, 1415−1424.

(23) Ellis, L. D.; Rorrer, N. A.; Sullivan, K. P.; Otto, M.; McGeehan, J. E.; Román-Leshkov, Y.; Wierckx, N.; Beckham, G. T. Chemical and biological catalysis for plastics recycling and upcycling. *Nat. Catal.* **2021**, *4*, 539−556.

(24) Coates, G. W.; Getzler, Y. D. Y. L. Chemical recycling to monomer for an ideal, circular polymer economy. *Nat. Rev. Mater.* **2020**, *5*, 501−516.

(25) Thiounn, T.; Smith, R. C. Advances and approaches for chemical recycling of plastic waste. *J. Polym. Sci.* **2020**, *58*, 1347−1364.

(26) Hong, M.; Chen, E. Y.-X. Chemically recyclable polymers: a circular economy approach to sustainability. *Green Chem.* **2017**, *19*, 3692−3706.

(27) Shi, C.; Reilly, L. T.; Phani Kumar, V. S.; Coile, M. W.; Nicholson, S. R.; Broadbelt, L. J.; Beckham, G. T.; Chen, E. Y.-X. Design principles for intrinsically circular polymers with tunable properties. *Chem* **2021**, *7*, 2896−2912.

(28) Kumar, A.; von Wolff, N.; Rauch, M.; Zou, Y.-Q.; Shmul, G.; Ben-David, Y.; Leitus, G.; Avram, L.; Milstein, D. Hydrogenative Depolymerization of Nylons. *J. Am. Chem. Soc.* **2020**, *142*, 14267−14275.
(29) Kamimura, A.; Shiramatsu, Y.; Kawamoto, T. Depolymerization of polyamide 6 in hydrophilic ionic liquids. *Green Energy Environ.* **2019**, *4*, 166−170.
(30) Alberti, C.; Figueira, R.; Hofmann, M.; Koschke, S.; Enthaler, S. Chemical Recycling of End-of-Life Polyamide 6 via Ring Closing Depolymerization. *ChemistrySelect* **2019**, *4*, 12638−12642.
(31) Chen, J.; Li, Z.; Jin, L.; Ni, P.; Liu, G.; He, H.; Zhang, J.; Dong, J.; Ruan, R. Catalytic hydrothermal depolymerization of nylon 6. *J. Mater. Cycles Waste Manage.* **2010**, *12*, 321−325.
(32) Kamimura, A.; Yamamoto, S. An Efficient Method To Depolymerize Polyamide Plastics: A New Use of Ionic Liquids. *Org. Lett.* **2007**, *9*, 2533−2535.
(33) Bockhorn, H.; Donner, S.; Gernsbeck, M.; Hornung, A.; Hornung, U. Pyrolysis of polyamide 6 under catalytic conditions and its application to reutilization of carpets. *J. Anal. Appl. Pyrolysis* **2001**, *58*−*59*, 79−94.
(34) Mihut, C.; Captain, D. K.; Gadala-Maria, F.; Amiridis, M. D. Review: Recycling of nylon from carpet waste. *Polym. Eng. Sci.* **2001**, *41*, 1457−1470.
(35) Czernik, S.; Elam, C. C.; Evans, R. J.; Meglen, R. R.; Moens, L.; Tatsumoto, K. Catalytic pyrolysis of nylon-6 to recover caprolactam. *J. Anal. Appl. Pyrolysis* **1998**, *46*, 51−64.
(36) Shi, C.; Li, Z.-C.; Caporaso, L.; Cavallo, L.; Falivene, L.; Chen, E. Y.-X. Hybrid monomer design for unifying conflicting polymerizability, recyclability, and performance properties. *Chem* **2021**, *7*, 670−685.
(37) Liu, Y.; Wu, J.; Hu, X.; Zhu, N.; Guo, K. Advances, Challenges, and Opportunities of Poly(γ-butyrolactone)-Based Recyclable Polymers. *ACS Macro Lett.* **2021**, *10*, 284−296.
(38) Shi, C.; Clarke, R. W.; McGraw, M. L.; Chen, E. Y.-X. Closing the "One Monomer−Two Polymers−One Monomer" Loop via Orthogonal (De)polymerization of a Lactone/Olefin Hybrid. *J. Am. Chem. Soc.* **2022**, *144*, 2264−2275.
(39) Barnes, C. *Nylon 4-Development and Commercialization*; Lenzinger Ber, 1987; pp 62−66.
(40) Grewal, J.; Khare, S. K. 2-Pyrrolidone synthesis from γ-aminobutyric acid produced by Lactobacillus brevis under solid-state fermentation utilizing toxic deoiled cottonseed cake. *Bioprocess Biosyst. Eng.* **2017**, *40*, 145−152.
(41) De Schouwer, F.; Claes, L.; Claes, N.; Bals, S.; Degreve, J.; De Vos, D. E. Pd-catalyzed decarboxylation of glutamic acid and pyroglutamic acid to bio-based 2-pyrrolidone. *Green Chem.* **2015**, *17*, 2263−2270.
(42) Tanielyan, S. K.; More, S. R.; Augustine, R. L.; Tosukhowong, T.; Ozmeral, C.; Roffi, K.; Shmorhun, M.; Glas, J. Hydrogenation of Succinimide to 2-Pyrrolidone Over Solid Catalysts. *Top. Catal.* **2014**, *57*, 1582−1587.
(43) Yamano, N.; Kawasaki, N.; Takeda, S.; Nakayama, A. Production of 2-Pyrrolidone from Biobased Glutamate by Using Escherichia coli. *J. Polym. Environ.* **2013**, *21*, 528−533.
(44) Yamano, N.; Kawasaki, N.; Ida, S.; Nakayama, A. Biodegradation of polyamide 4 in seawater. *Polym. Degrad. Stab.* **2019**, *166*, 230−236.
(45) Tachibana, K.; Hashimoto, K.; Yoshikawa, M.; Okawa, H. Isolation and characterization of microorganisms degrading nylon 4 in the composted soil. *Polym. Degrad. Stab.* **2010**, *95*, 912−917.
(46) Yamano, N.; Nakayama, A.; Kawasaki, N.; Yamamoto, N.; Aiba, S. Mechanism and Characterization of Polyamide 4 Degradation by Pseudomonas sp. *J. Polym. Environ.* **2008**, *16*, 141−146.
(47) Tachibana, K.; Hashimoto, K.; Tansho, N.; Okawa, H. Chemical modification of chain end in nylon 4 and improvement of its thermal stability. *J. Polym. Sci., Part A: Polym. Chem.* **2011**, *49*, 2495−2503.
(48) Russo, S.; Casazza, E. 4.14—Ring-Opening Polymerization of Cyclic Amides (Lactams). In *Polymer Science: A Comprehensive Reference*; Matyjaszewski, K., Möller, M., Eds.; Elsevier: Amsterdam, 2012; pp 331−396.
(49) Bour, E. H. J. P.; Warnier, J. M. M.; Brouwers, J. A. L. Preparation of poly-2-pyrrolidone with N-(2-caprolactim)-caprolactam accelerator. U.S. Patent 4,362,862 A, 1982.
(50) Roda, J.; Brozek, J.; Králícek, J. Polymerization of lactams, 37. Isolation and characterization of alkali carboxylates of 2-pyrrolidone. *Makromol. Chem., Rapid Commun.* **1980**, *1*, 165−169.
(51) Schirawski, G. Untersuchungen zur anionischen polymerisation von pyrrolidon. *Makromol. Chem.* **1972**, *161*, 57−68.
(52) Hall, H. K. Polymerization and Ring Strain in Bridged Bicyclic Compounds. *J. Am. Chem. Soc.* **1958**, *80*, 6412−6420.
(53) Sangroniz, A.; Zhu, J.-B.; Tang, X.; Etxeberria, A.; Chen, E. Y.-X.; Sardon, H. Packaging materials with desired mechanical and barrier properties and full chemical recyclability. *Nat. Commun.* **2019**, *10*, 3559.
(54) Winnacker, M.; Neumeier, M.; Zhang, X.; Papadakis, C. M.; Rieger, B. Sustainable Chiral Polyamides with High Melting Temperature via Enhanced Anionic Polymerization of a Menthone-Derived Lactam. *Macromol. Rapid Commun.* **2016**, *37*, 851−857.
(55) Amorín, M.; Castedo, L.; Granja, J. R. Self-Assembled Peptide Tubelets with 7 Å Pores. *Chem.—Eur. J.* **2005**, *11*, 6543−6551.
(56) Amorín, M.; Castedo, L.; Granja, J. R. New Cyclic Peptide Assemblies with Hydrophobic Cavities: The Structural and Thermodynamic Basis of a New Class of Peptide Nanotubes. *J. Am. Chem. Soc.* **2003**, *125*, 2844−2845.
(57) Miyake, G. M.; DiRocco, D. A.; Liu, Q.; Oberg, K. M.; Bayram, E.; Finke, R. G.; Rovis, T.; Chen, E. Y.-X. Stereospecific Polymerization of Chiral Oxazolidinone-Functionalized Alkenes. *Macromolecules* **2010**, *43*, 7504−7514.
(58) Lin, Y.; Bilotti, E.; Bastiaansen, C. W. M.; Peijs, T. Transparent semi-crystalline polymeric materials and their nanocomposites: A review. *Polym. Eng. Sci.* **2020**, *60*, 2351−2376.
(59) Bellinger, M. A.; Ng, C.-W. A.; Macknight, W. J. Effects of water on the mechanical relaxation in polyamide 4. *Acta Polym.* **1995**, *46*, 361−366.
(60) Zhu, J.-B.; Watson, E. M.; Tang, J.; Chen, E. Y.-X. A synthetic polymer system with repeatable chemical recyclability. *Science* **2018**, *360*, 398−403.
(61) PA6. https://designerdata.nl/materials/plastics/thermoplastics/polyamide-6 (accessed August 9, 2021).
(62) Hashimoto, K.; Sumitomo, H.; Washio, A. Preparation of monodisperse hydrophilic polyamide by anionic polymerization of bicyclic oxalactam. *J. Polym. Sci., Part A: Polym. Chem.* **1989**, *27*, 1915−1923.
(63) Hashimoto, K.; Sumitomo, H. Synthesis and Polymerization of an Optically Active Bicyclic Oxalactam. A Novel Hydrophilic Polyamide Membrane Prepared from (+)-(1R,5S)-8-Oxa-6-azabicyclo[3.2.1]octan-7-one. *Macromolecules* **1980**, *13*, 786−791.
(64) Sumitomo, H.; Hashimoto, K. Polymerization of Bicyclic Oxalactam. A Novel Polyamide Poly(tetrahydropyran-2,6-diyliminocarbonyl). *Macromolecules* **1977**, *10*, 1327−1331.
(65) Brown, J. R.; Ennis, B. C. Thermal Analysis of Nomex and Kevlar Fibers. *Text. Res. J.* **1977**, *47*, 62−66.
(66) Deming, T. J. 4.16—Ring-Opening Polymerization of Amino Acid *N*-Carboxyanhydrides. In *Polymer Science: A Comprehensive Reference*; Matyjaszewski, K., Möller, M., Eds.; Elsevier: Amsterdam, 2012; pp 427−449.
(67) Zhang, H.; Stephanopoulos, G. Co-culture engineering for microbial biosynthesis of 3-amino-benzoic acid in Escherichia coli. *Biotechnol. J.* **2016**, *11*, 981−987.
(68) Tang, J.; Chen, E. Y. X. Effects of Chain Ends on Thermal and Mechanical Properties and Recyclability of Poly( γ -butyrolactone). *J. Polym. Sci., Part A: Polym. Chem.* **2018**, *56*, 2271−2279.
(69) Towns, J.; Cockerill, T.; Dahan, M.; Foster, I.; Gaither, K.; Grimshaw, A.; Hazlewood, V.; Lathrop, S.; Lifka, D.; Peterson, G. D.; Roskies, R.; Scott, J. R.; Wilkins-Diehr, N. XSEDE: Accelerating Scientific Discovery. *Comput. Sci. Eng.* **2014**, *16*, 62−74.


https://doi.org/10.1021/jacs.1c12611
J. Am. Chem. Soc. XXXX, XXX, XXX−XXX